Est. 1984

ORIENTAL JOURNAL OF CHEMISTRY
An International Open Access, Peer Reviewed Research Journal

www.orientjchem.org

ISSN: 0970-020 X
CODEN: OJCHEG
2022, Vol. 38, No.(1):
Pg. 94-101

Sol Gel Synthesis and Characterization of Strontium Titanates

RAMANJEET KAUR[1]* and ANAND K TYAGI[2]

[1]Department of Applied Sciences, SBSSTC, I. K. Gujral Punjab Technical University, Kapurthala, 144603 (Punjab) India.
[2]Mahatma Gandhi Kashi Vidyapith, Varanasi (UP), India.
*Corresponding author E-mail: ramanjeetgill99@gmail.com, anandktyagi@gmial.com

http://dx.doi.org/10.13005/ojc/380111

(Received: January 01, 2022; Accepted: February 02, 2022)

ABSTRACT

Pure strontium titanates have been successfully fabricated in this work via sol gel route. The obtained powders were calcined at various temperatures and effects of calcination and sintering on phase development, crystallite size, lattice parameters, microstructure etc. were investigated by XRD and SEM techniques. The development of phase with temperature has been investigated using DTA/TG technique. The dielectric and electrical parameters were analyzed and effects of temperature and frequency variation on these parameters were studied.

Keywords: Sol gel, Synthesis, Strontium titanates, Characterization.

INTRODUCTION

Various types of materials have been investigated by different research groups as anode, cathode and electrolyte materials. From these, the oxides with perovskite structure draw considerable attention owing to their stability in reducing atmospheres, capability to withstand the sulfur contamination and carbon deposition etc. during SOFCs operation. Strontium titanates, lanthanum chromites and their doped forms are the emerging perovskite structured oxides that had been widely studied. Strontium titanate, both in pure and derived forms, is growing candidate as SOFC material as it offers many advantages over other materials like high stability in oxygen, carbon, and sulfur containing atmospheres[1-3], remarkably active for methane (CH_4) oxidation at high temperature in the absence of excess steam[3], high conductivity (mainly in doped forms)[4-11], stable dimensionally and chemically upon redox cycling etc.

EXPERIMENTAL

In this work we have synthesized pure strontium titanates via low temperature environment friendly sol gel technique. The main objective of the present work is to study the phase development with calcination at various temperatures; and other structural, micro-structural and electrical/dielectric properties. Furthermore the importance of these titanates for applications in SOFCs will be analyzed.

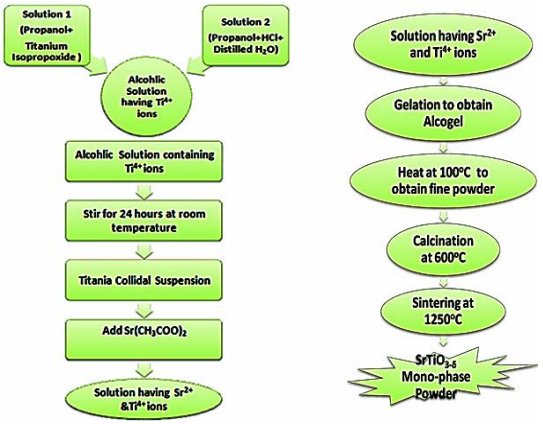

Fig. 1. Flow chart for synthesis of $SrTiO_{3-\delta}$samples

$SrTiO_{3-\delta}$; STO has been synthesized via sol gel route[12] using strontium acetate $\{Sr(CH_3COO)_2\}$, titanium tetra isopropoxide $\{Ti(OC_3H_7)_4\}$; both from Alfa AesarTM, as metal precursors; hydrochloric acid (HCl) as catalyst; propanol and distilled water as solvents using the metallurgical reaction (1).

$$Sr(CH_3COO)_2 + Ti(OC_3H_7)_4 \rightarrow SrTiO_{3-\delta} + \quad (1)$$

The powders obtained after drying and crushing the alcogel were calcined at 600°C, 800°C, 920°C, 1000°C, 1100°C, 1150°C and 1250°C for 2 h to obtain mono-phase powders. The calcinations were done in High Temperature Muffle Furnace with power rating 5.0 KW and 220 Volt ac supply at SBSSTC research lab. The powders were pelletized, calcined at 600°C to expel the binder and then, further sintered at 1250°C for two hours. The flow chart representing the whole experimental procedure is given in Fig.1. The obtained samples were analyzed using DTA/TG, XRD, SEM, LCR Hitester techniques.

DTA/TGA/DTG analysis was carried out using EXSTAR TG/DTA 6300. The nitrogen atmosphere (200 mL/min) was kept during all the experiments. The amount of the sample used was 10.540 mg. The alumina powder (Al_2O_3) was used as reference material. The heating of sample was done from 35°C to 1200°C temperature. X-ray diffraction of $SrTiO_{3-\delta}$ ceramic samples obtained after calcination at various temperatures was carried out using a XPERT-PRO X-ray diffractometer; type 0000000011023505. The machine was operated with a beam current of generator settings 40mA and 45kV power. The radiation used was Kα1 having wavelength 1.54060Å using Cu as target and nickel metal was used as β filter. The goniometer used was PW3050/60. The micro structural properties were investigated using JSM-6510 instrument. The instrument provides various magnification powers e. g. 5000xs, 10000xs; 20000xs etc. and operates at accelerating voltage 15kV. The sample thickness used in SEM analysis is lesser than 2mm. The samples were coated with gold layer of thickness ~100Å to avoid the charging effects using Auto Fine Coater at 20A for 40 sec. The impedance analysis was carried out on SOLARTRON (SI1260) impedance analyzer. Various parameters like real - imaginary components of impedance and relative permittivity were measured by the instrument at various temperatures i.e. at room temperature and from 48°C to 400°C. The frequency range used in the analysis was from 100 Hz to 1 MHz.

RESULTS AND DISCUSSION

Thermal Analysis

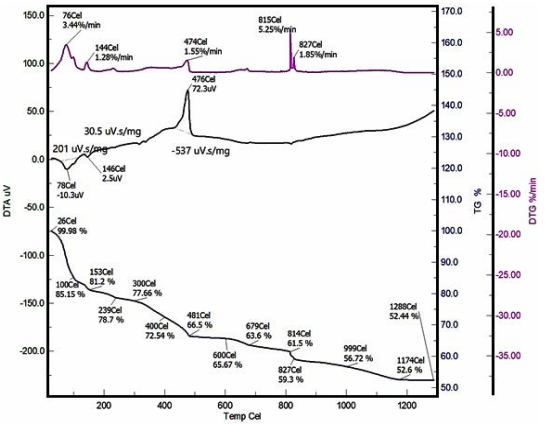

Fig. 2. DTA/TG/DTG thermo-gram for uncalcined powder of $SrTiO_{3-\delta}$sample

DTA/TG/DTG thermo-grams obtained for uncalcined powder of $SrTiO_{3-\delta}$ are shown in Fig. 2. The curve can be divided mainly in three parts. First part of TG curve corresponds to heavy weight loss; 99.98% to 78.7% in temperature range 26°C to 239°C having two endothermic peaks at 78°C and 146°C. This weight loss is due to the evaporation of some remainders of solvents with rise in the temperature. The second part of TG curve corresponds to weight loss from 78.7% to 61.5% in the temperature range from 239°C to 814°C and exothermic peak at 476°C due to decomposition of organic compounds and nitrates. The third part of

the curve corresponds to weight loss from 59.3% to 52.44% in the temperature range from 815°C to 1288°C with two small endothermic peaks at 815°C and 827°C. This region of thermo-gram corresponds to the development of $SrTiO_3$ phase[12-14].

XRD Analysis

The XRD peak patterns for $SrTiO_{3-\delta}$ powders calcined at different temperatures 600°C, 800°C, 920°C, 1000°C, 1100°C, 1150°C and 1250°C are shown in Fig. 3. It can be depicted from the figure that XRD peaks are sharp; well defined and indexing of peaks has been done considering the cubic symmetry of structure using mathematical method[15]. $Sr(OH)_2$, $SrCO_3$, TiO_2 and SrO are present as impurity or intermediate phases at lower temperatures whereas XRD peak patterns at temperature 1250°C has peaks mainly corresponding to $SrTiO_{3-\delta}$.

The variation in the amounts of impurities and required phase with temperature is given in Fig. 4. Herein, the graphs have been plotted using normalized intensities. The intensities of peaks of impurity and intermediate phases have been normalized by 2778, the intensity of (101) peak of TiO_2, which is highest among all peaks of impurity and intermediate phases, whereas, intensities of all the peaks of the desired compound i.e. $SrTiO_{3-\delta}$, have been normalized by 14807, the intensity of (110) reflection of $SrTiO_{3-\delta}$ at 1100°C temperature, which is the highest value of intensity in the XRD pattern.

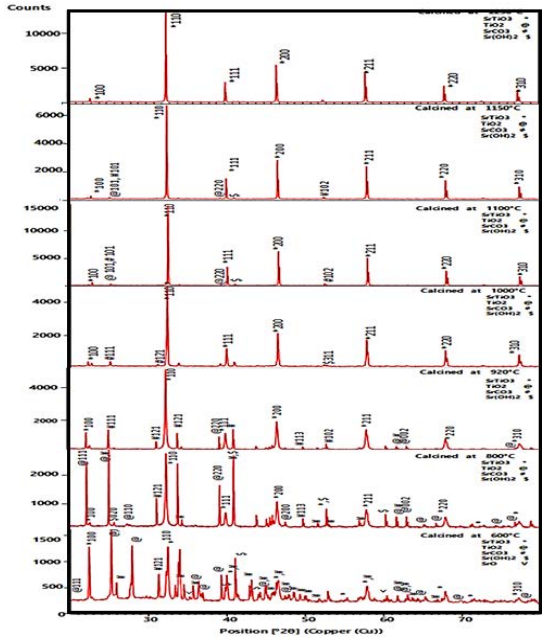

Fig. 3. X-ray Diffraction peaks for $SrTiO_{3-\delta}$ calcined at various temperatures

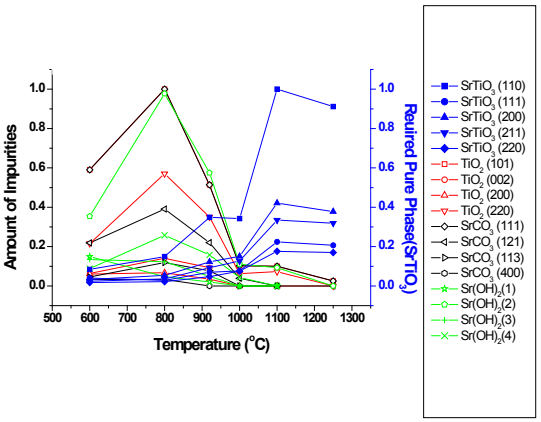

Fig. 4. Variation of amount of $SrTiO_{3-\delta}$ phase and intermediate phases with rise in the temperature

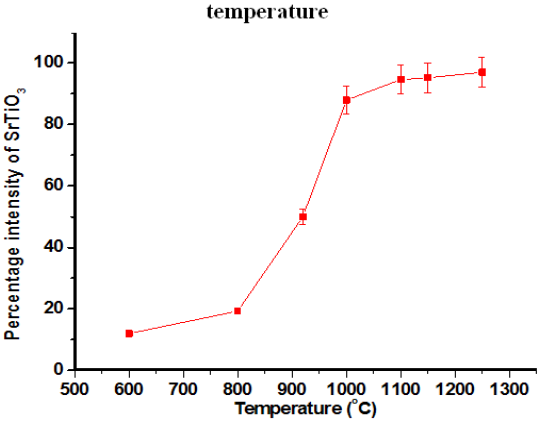

Fig. 5. Variation of percentage amount of $SrTiO_{3-\delta}$ phase with temperature

It can be easily inferred from the graph that the intensiy of the desired $SrTiO_{3-\delta}$ phase increases with rise in the temperature whereas that of intermediate phases and impuritiesi.e. $SrCO_3$, TiO_2, $Sr(OH)_2$ decreases with rise in the temperature. The percentage amount of the required $SrTiO_{3-\delta}$ phase has been calculated at various temperatures using the relation (2). The graphical variation of percentage amount with temperature has been shown in Fig. 5 which clearly indicates that amount of $SrTiO_{3-\delta}$ phase increases with rise in temperature; with highest value 97% for samples sintered at 1250°C.

$$X(SrTiO_{3-\delta}) = \frac{I(SrTiO_{3-\delta})}{I(SrTiO_{3-\delta}) + I(SrCO_3) + I(TiO_2) + I\{Sr(OH)_2\}} \times 100\% \quad (2)$$

Here X ($SrTiO_{3-\delta}$) is the percentage amount of $SrTiO_{3-\delta}$ phase and I($SrTiO_{3-\delta}$), I($SrCO_3$), I(TiO_2) and I{$Sr(OH)_2$} are intensities of $SrTiO_{3-\delta}$, $SrCO_3$, TiO_2 and $Sr(OH)_2$ phases obtained from XRD diffraction peaks respectively.

Lattice parameter 'a' values for $SrTiO_{3-\delta}$ at various temperatures, as calculated using mathematical method for cubic crystals[15] are given in Table 1. For cubic systems, relation between Θ, wavelength (λ), lattice parameters and miller indices (h k l) is given by equation (3).

$$(a)^2 = \frac{\lambda^2}{4(\sin\theta)^2} \quad [(h^2 + k^2 + l^2)] \qquad (3)$$

Here λ = 1.5406Å. Clearly, as depicted by Table (1), the lattice parameter 'a' decreases with rise in temperature and the average value of 'a' is determined to be 3.9087Å which is very close to theoretical value of 'a' 3.91Å[16]. The crystallite sizes, as calculated for $SrTiO_{3-\delta}$ samples obtained after calcination at various temperatures, using the Scherrer's equation are given in Table 1[17]. These have been determined for (110), (211) and (310) reflection peaks in the XRD patterns. Clearly, as depicted from Table 1, the crystallite size for the reflection peaks (110), (211) and (310) increases with temperature up to 1100°C, then it slightly decreases at temperature 1150°C; then again it increases up to 1250°C. The increase in crystallite size suggests the ongoing process of crystallization with increase in the temperature. The slight crystallite size decrement at 1150°C may be because of inter-planar shift of atoms.

Table 1: Variation of crystallite size and lattice parameter for $SrTiO_{3-\delta}$ with temperature

Temperature (°C)	Crystallite Size (nm)			Lattice Parameter (Å)	
	(110)	(310)	(211)	Experimental value	Measurement error
600	54.93	41.48	44.47	3.9222	-0.0122
800	53.99	30.21	35.18	3.9072	0.0028
920	56.97	35.04	44.78	3.9035	0.0065
1000	81.09	74.21	88.93	3.9192	0.0092
1100	139.04	132.71	140.04	3.9023	-0.0077
1150	128.86	126.91	127.99	3.9021	-0.0079
1250	135.42	137.79	140.29	3.8980	-0.0120

SEM Analysis

SEM analysis was carried out for both, calcined (at 600°C) and sintered (at 1250°C), pure $SrTiO_{3-\delta}$ pellets and effect of sintering on microstructure and grain size distribution was studied. SEM microstructures of $SrTiO_{3-\delta}$ sample obtained after calcination at 600°C for 2 h are given in Fig. 6 (a and b) whereas the Fig. 6 (c) depicts the microstructure of pure $SrTiO_{3-\delta}$ sample obtained after 2 h sintering of pellets at 1250°C. It can be revealed that microstructure of $SrTiO_{3-\delta}$ samples obtained after calcination at 600°C was almost homogeneous but a little cluster formation and merged grain boundaries were observed. The grains were polyhedral shaped and nano sized; from 407nm to 972nm. Whereas the pure $SrTiO_{3-\delta}$ samples obtained after sintering the pellets at 1250°C had homogeneous microstructure with well developed, small angular grains having well defined, smooth and clear grain boundaries, edges, corners, faces having cubiodal shapes. The sintered $SrTiO_{3-\delta}$ samples showed good sinterabiltiy with marginal inter-granular porosity and average grain size was 728nm. Thus sintering led to well developed microstructure for the synthesized samples. The sol gel method produces very fine powders and furthermore, the sintering temperature employed here is also low (1250°C); which lead to nano-sized ceramic samples[18-19].

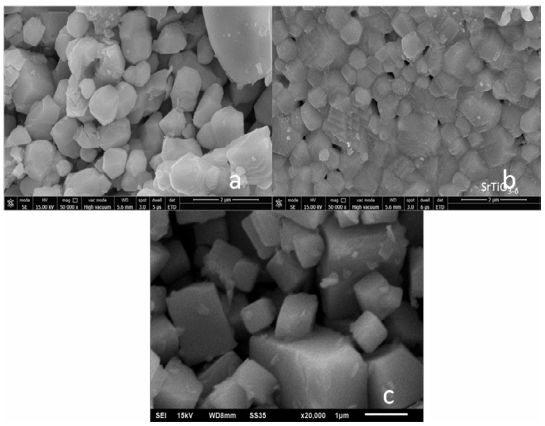

Fig. 6. SEM images of $SrTiO_{3-\delta}$ sample obtained after (a and b) caclination at 600°C (c) sintering at 1250°C

Electrical and dielectric characterization

The dependence of ε_{real} on frequency for STO sample at room temperature is shown in Fig. 7(a). The dielectric constant decreases very sharply up to frequency 1KHz and then remains almost constant above that[20-21]. The variations of dielectric constant with temperature ranging from 50 to 400°C at frequencies 10KHz and 100KHz for $SrTiO_{3-\delta}$; STO sample is shown in Fig. 7(b). The dielectric constant remains almost constant up to a certain temperature and then, increases rapidly with

increasing temperature which may be due to space charge polarization[22]. The high values of dielectric constant at room temperature for this STO sample may be attributed to the presence of all kinds of polarizations at room temperature which can lead to irregular increase in the permittivity[23-24]. The dielectric constant value for pure sample was measured to be ~64 at frequency 1KHz and temperature 400°C.

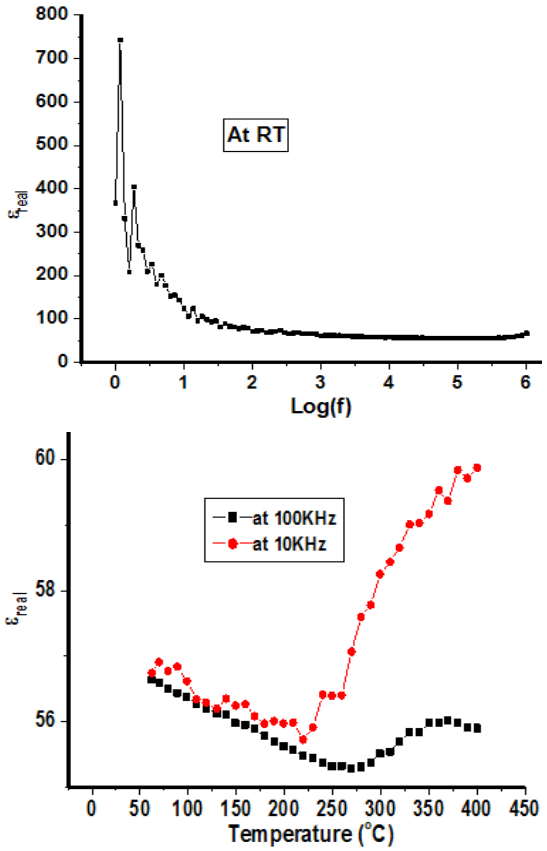

Fig. 7. Variation of dielectric constant (a) with log (frequency) at room temperature (RT) (b) with temperature at frequencies 10 KHz and 100 KHz for $SrTiO_{3-\delta}$ sample

Figure 8 shows the frequency dependence of imaginary dielectric constant (ε_{img}) for pure $SrTiO_3$ (STO) sample. ε_{img} shows the similar trends as that of ε_{real} i.e. increase with temperature and decrease with frequency. There is no loss peak in the whole frequency spectrum of ε_{img}. The values of ε_{img} are high only at low frequencies (below 1KHz) and at high temperature (300°C to 400°C) owing to the interfacial build up of the free charges either within the sample; termed as Maxwell Wagner (MW) polarization[25] or between electrodes and sample; termed as Space Charge (SC) polarization. The imaginary component of dielectric constant (ε_{img}) for pure undoped sample is 0.340 at frequency 10KHz and temperature 108°C.

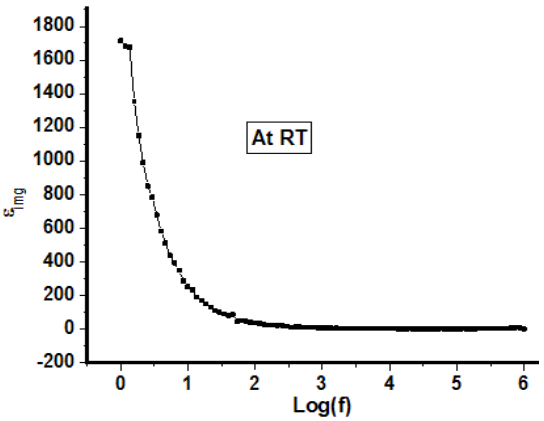

Fig. 8. Variation of imaginary part of dielectric constant (ε_{img}) with log (frequency) at RT for $SrTiO_{3-\delta}$ sample

The frequency variation of loss tangent factor (tanδ) for STO sample at room temperature (RT) is shown in Fig. 9(a). While the Fig. 9(b) depicts the temperature dependence of loss factor at 1000KHz and 100KHz frequencies from 50 to 400°C. From all these plots, the decrease in loss factor with frequency and increase in it with temperature can be revealed easily.

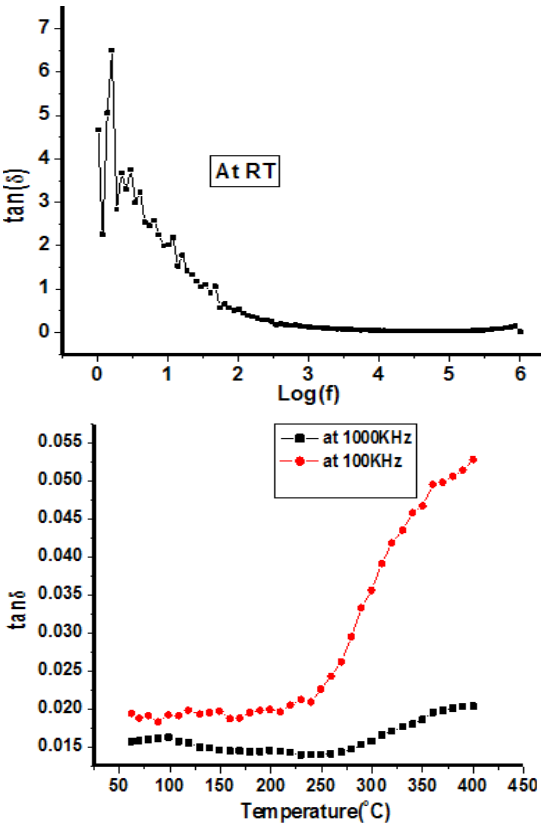

Fig. 9. Variation of loss tangent factor (a) with log (frequency) at RT (b) with temperature at various frequencies for $SrTiO_{3-\delta}$ sample

The dielectric loss for the $SrTiO_{3-\delta}$ measured at temperature below 250°C was very small e.g. 0.00604 at frequency 10KHz and temperature 108°C; but by increasing the temperature from 250°C to 400°C, the dielectric loss value increased.

The variation trends of ac conductivity (σ_{ac}) with frequency at room temperature (RT) and with temperature at 10KHz and 100KHz frequencies for synthesized STO sample are included in Fig. 10(a) and 10(b) respectively. It can be easily depicted that ac conductivity for the $SrTiO_{3-\delta}$ sample was almost constant at lower frequencies; while at higher temperatures and frequencies there was sharp enhancement in ac conductivity acquiring approximately 4.6 x 10^{-4} value at frequency 1MHz and temperature 400°C; this increase may be due to the strong hopping mechanism[26].

Figure 11(a) includes the change in real part of impedance (Z') for STO sample with frequency at room temperature, 108, 209, 309 and 400°C respectively. The decrement in Z' with frequency as well as with temperature can be easily depicted from the figure. The decrease in Z" with rise in temperature is very clear at low frequencies in Fig. 11(a) whereas Z′ values at various temperatures coincide at high frequency. The decrease of impedance with temperature reveals the fact that synthesized materials possess negative temperature coecient of resistance. The rise in temperature reduces the barrier which in turn leads to increase in ac conductivity and thus decrement in Z′ e.g. the real impedance value for the pure sample reduced from 582883 (at room temperature) to 251586 (at 400°C); both determined at frequency 1KHz. Fig. 11(b) includes the frequency dependence of imaginary component of impedance (Z") for pure STO sample at various temperatures. It can be easily depicted from the curves that Z" values show a maximum value at low frequency which decreases with temperature. The values of Z" merge at high frequencies, as clearly visible from the plots; the space charge build up within the sample may be reason for that[27-29]. Fig. 12 shows the Cole-Cole plots of STO sample at room and other higher temperatures. The grain effects in the samples are indicated by presence of semicircle; furthermore, the decrement in semicircle radius with increasing temperature can be observed; inferring the decrease in the resistivity with rise of temperature[26].

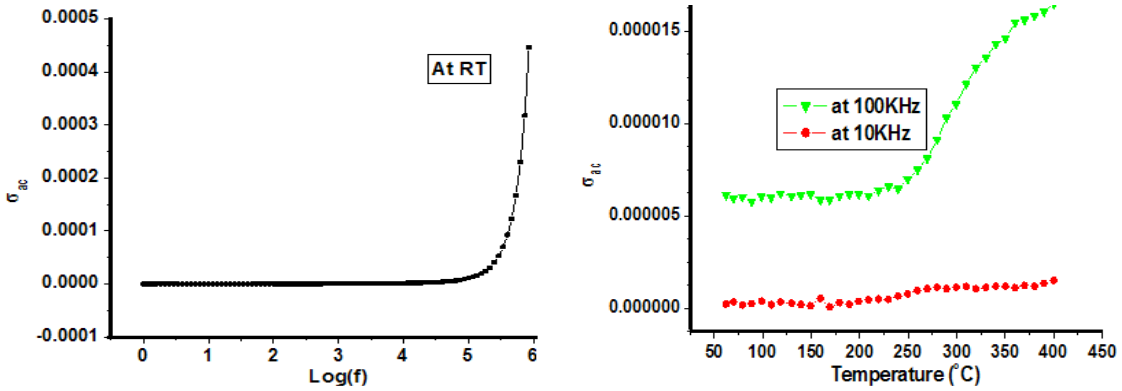

Fig. 10. Variation of ac conductivity (σ_{ac}) (a) with log (frequency) at RT (b) with temperature at frequencies 10KHz and 100KHz for STO sample

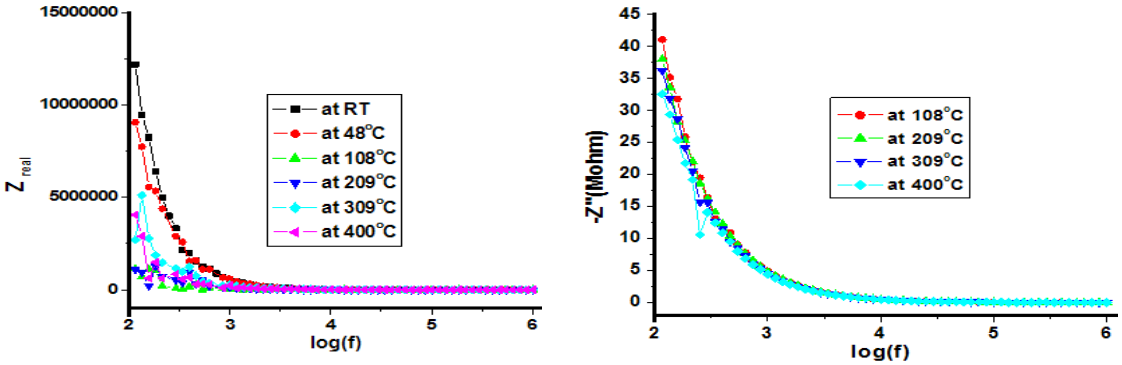

Fig. 11. Variation of (a) real component of impedance (Z_{real}) with log (frequency) at RT and at higher tempertaures (b) imaginary component of impedance (Z'') with log (frequency) at various temperatures for STO sample

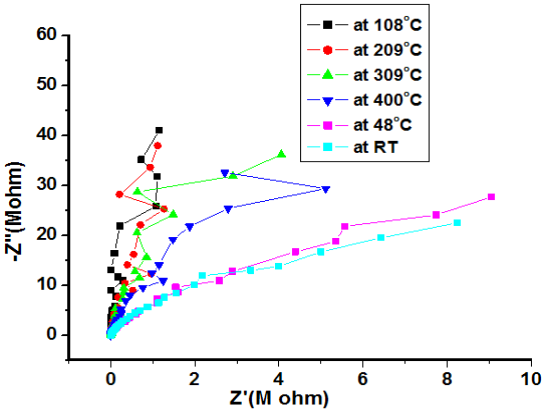

Fig. 12. Cole-Cole plots between real and imaginary part of impedance at room and higher temperatures for STO sample

CONCLUSION

Here, in this work, we have successfully synthesized the strontium titanates with required cubic structure employing novel sol gel technique. The impurities in the powders go on decreasing with increase in calcination temperature and phase pure samples have been obtained after sintering at 1250°C. The obtained samples were phase pure, homogeneous and having well-developed morphology as revealed by XRD and SEM techniques. The synthesized samples possess good electrical and dielectric properties which make this material suitable for applications in SOFCs.

ACKNOWLEDGEMENT

One of the authors Ms. Ramanjeet Kaur highly acknowledges IKGPTU (Inder Kumar Gujral Punjab Technical University), Kapurthala, Punjab, India for providing facilities in this course. The authors are also very thankful to TEQIP, MHRD/ World Bank Project, IIC, I.I.T. Roorkee, MRC, MNIT Jaipur, Thapar University, Patiala and S B S State Technical Campus, Ferozepur for help and support in this whole work.

Conflict of interest

The author declare that we have no conflict of interest.

REFERENCES

1. R., Mukundan.; E. L., Brosha.; F. H., Garzon, *Electrochem. Solid-State Lett.*, **2004**, *7*, A5–A7.
2. Z., Cheng.; S., Zha.; M., Liu, *Journal of Electrochemical Society.*, **2006**, *153*, A1302–A1309.
3. J. C., Ruiz-Morales.; J., Canales-Vázquez.; C., Savaniu.; D., Marrero López.; W., Zhou.; J. T. S., Irvine, *Nature.*, **2006**, *439*, 568.
4. S., Hui.; A., Petric, *J. Eur. Ceram. Soc.*, **2002**, *22*, 1673–1681.
5. S., Hui.; A., Petric, *J. Electrochem. Soc.,* **2002**, *149*, J1–J10.
6. Q. X., Fu.; F., Tietz.; D., Stover, *J. Electrochem. Soc.*, **2006**, *153*, D74-D83.
7. J. C., Ruiz-Morales.; J., Canales-Vázquez.; C., Savaniu.; D., Marrero López.; W., Zhou; J. T. S., Irvine.; *Nature.*, **2006**, *439*, 568.
8. S. W., Tao.; J. T. S., Irvine.; *Nat. Mater.*, **2003**, *2*, 320.
9. S. W., Tao.; J. T. S., Irvine.; *J. Electrochem. Soc.*, **2004**, *151*, A252-A259.
10. H., Yang.; T., Zhong.; Z., Chen.; X., Wang; N., Ai.; Ceramics International., **2022**.
11. D., Kim.; I., Jeong.; K. J., Kim.; K. T., Bae.; D. Kim.; J. Koo.; H., Yu.; K. T., Lee; *Journal of Korean Ceramic Society.*, **2022**.
12. A., Rocca.; A., Licciulli.; M., Politi.; D., Diso.; International Scholarly Research Network Ceramics., **2012**.
13. B., Li.; C., Wang.; C., Liu.; W., Zhong.; R., *An, Materials Letters.*, **2012**, *75*, 207–210.
14. S., Ueno.; K., Nakashima.; Y. Sakamoto.; S., Wada.; *Nanomaterials.*, **2015**, *5*, 386-397.
15. Laboratory Module, Indexing X-ray Diffraction Patterns.
16. L., Zhang.; T., Tosho.; N., Okinaka.; T., Akiyama, *Mater. Trans.*, **2007**, *48*, 2088-2093.
17. B. D.,Cullity.; Elements of X-ray Diffraction Addison-Wesley., **1978**.
18. L., Zhang.; T., Tosho.; N., Okinaka.; T., Akiyama.; *Materials Transactions.,* **2007**, *48*(8), 2088-2093.
19. H. C., Wang.; W. C., Lei.; W. B., Su.; J., Liu.; Y., Sun.; H., Peng.; L. M., Mei.; *J. Am. Ceram. Soc.*, **2011**, *94*, 838–842.

20. A., Verma.; O. P., Thakur.; C., Prakash.; T. C., Goel.; R. G., *Mendiratta, Mater. Sci. Eng.*, **2005**, B116.
21. T., Badapanda.; R. K., Harichandan.; A., Mishra.; S., Anwar, *J. Adv. Dielectr.*, **2013**, *3*, 1350013.
22. P., Abhijit.; B., Amitabha.; *J. Mater. Sci.: Mater. Electron.*, **2013**, *24*, 1855–1862.
23. X., Wang.; B., Zhang.; L., Xu.; Y., Hu.; G., Shen.; L., Sun.; *Sci. Rep.,* **2017**, *7*, 8517.
24. A., Ray.; B., Behera.; T., Basuy.; S., Vajandarz.; S. K., Satpathy.; Nayak, *J. Adv. Dielectr.*, **2018**, *85*, 1850031.
25. S., Kumar.; K. B. R., Varma, *Solid State Commun.*, **2008**, *147*, 457–460.
26. K. C. B., Naidu.; T. S., Sarmash.; T., Subbarao; *Int. J. Eng. Res. Technol.,* **2014**, 3.
27. T., Badapanda.; R. K., Harichandan.; S. S., Nayak.; A., Mishra.; S., Anwar.; T., Badapanda.; *Process. Appl. Ceram.*, **2014**, *8*, 145–153.
28. S., Sahoo.; U., Dash.; S. K. S., Parashar.; S. M., *All, J. Adv. Ceram.*, **2013**, *2*, 291–300.
29. A., V., Murugan.; S. C., Navale.; V., Ravi, *Materials Letters.*, **2006**, *60*, 1023–1025.